International Journal of Solids and Structures 96 (2016) 126–135

Contents lists available at ScienceDirect

International Journal of Solids and Structures

journal homepage: www.elsevier.com/locate/ijsolstr

Static and dynamic behavior of porous elastic materials based on micro-dilatation theory: A numerical study using the MLPG method

J. Sladek[a,*], V. Sladek[a], M. Repka[a], P.L. Bishay[b]

[a] Institution of Construction and Architecture, Slovak Academy of Sciences, 84503 Bratislava, Slovakia
[b] College of Engineering and Computer Science, California State University, Northridge, CA, United States

ARTICLE INFO

Article history:
Received 26 May 2015
Revised 8 June 2016
Available online 14 June 2016

Keyword:
Porous material
Cowin-Nunziato model
Local integral equations
Moving least square method
Micro-dilatation
Stress intensity factor (SIF)

ABSTRACT

A meshless local Petrov-Galerkin (MLPG) model of porous elastic materials based on micro-dilatation theory by Cowin and Nunziato (1983) is developed. . This theory describes properties of homogeneous elastic materials with voids free of fluid. The primal fields (mechanical displacements, and change in matrix volume fraction which is also called micro-dilatation) are coupled in the constitutive equations. The governing differential equations are satisfied in the weak form on small circular subdomains for 2D problems. Only one node is lying at the center of each subdomain spread on the analyzed domain. A Heaviside step function is applied as test functions in the weak-form to derive local integral equations on subdomains. The spatial variation of the displacements and micro-dilatation are approximated by the moving least-squares (MLS) scheme. After performing the spatial integrations, a system of ordinary differential equations for certain nodal unknowns is obtained.

1. Introduction

Recent advances in techniques for foaming metals and ceramics have led to their intense study, extending the understanding of such materials (Ashby et al., 2000; Colombo and Scheffler, 2005). There are number of theories about mechanics of porous materials. One of them is Biot consolidation theory for modeling fluid-saturated porous solids (Biot and Willis, 1957). Typically, these theories reduce to classical elasticity when the pore fluid is absent, and Biot consolidation theory cannot be applied for materials with voids free of fluid. Therefore, Cowin and Nunziato (1983) proposed a new theory to describe properties of homogeneous elastic materials with voids free of fluid. In that model, a certain volume fraction field of pores is introduced as an unknown function. This new function of volumetric density significantly influences the stress–strain state. The theory is founded on the balance of energy, where the presence of pores involves additional degree of freedom. Cowin-Nunziato theory (also known as micro-dilatation theory) has been successfully applied to many problems with special geometries under particular boundary conditions (see, for example, Adkin et al., 1977; Chandrasekharaiah, 1987; Scalia and Sumbatyan, 2000; Scalia, 2002; and recently Ramézani et al., 2012; Ramézani and Jeong, 2015) and showed good agreement with both experimental data and physical conclusions. The theory can also be utilized for modeling cracks in porous materials (Ciarletta et al., 2003). The solution of general boundary value problems for solids with voids requires advanced numerical methods due to coupling of mechanical displacements and the change in matrix volume fraction in the constitutive equations.

In recent years, meshless methods have become very popular computational tools for solving many engineering problems. This is due to their high adaptivity and low costs to prepare input and output data for numerical analyses. A meshless method can be obtained from a weak-form formulation on either the global domain or a set of local subdomains. In the global formulation, background cells are required for the integration of the weak-form. In methods based on local weak-form formulation, no background cells are required and therefore they are often referred to as “truly meshless methods” . The meshless local Petrov-Galerkin (MLPG) method is a fundamental base for the derivation of many meshless formulations since the trial and test functions can be chosen from different functional spaces (Atluri, 2004). The MLPG method with a Heaviside step function as the test functions (Atluri and Shen, 2002; Atluri et al., 2003) is the simplest and most reliable technique, which is frequently applied to solve two-dimensional (2-D) homogeneous and continuously non-homogeneous elastic solids (Sladek et al., 2004, 2008d, 2009) and for 3-D problems in homogeneous and isotropic solids under static or dynamic loads (Han and Atluri, 2004a, 2004b; Sladek et al., 2009). The method has also been successfully applied to coupled problems (Sladek et al., 2007,

* Corresponding author. Fax: +421-2-54773548.
E-mail addresses: sladek@savba.sk (J. Sladek), peter.bishay@csun.edu (P.L. Bishay).

http://dx.doi.org/10.1016/j.ijsolstr.2016.06.016
0020-7683/

2008c, 2014; Shirzadi et al., 2013), and plate/shell problems (Sladek et al., 2008a,b) and review of the MLPG has been published recently (Sladek et al., 2013).

In this paper, the MLPG method is applied to solving two-dimensional boundary value problems in porous elastic solid described by the micro-dilatation (Cowin-Nunziato) theory. The nodal points are introduced and distributed over the analyzed domain, each of which is surrounded by a small circle for 2-D problems. The weak-form on small subdomains with a Heaviside step function as the test functions is applied to derive local integral equations. The spatial variations of displacements and change in matrix volume fraction are approximated by the moving least-squares (MLS) scheme. After performing the spatial integrations, a system of ordinary differential equations for certain nodal unknowns is obtained. The backward finite difference method is applied to the approximation of the diffusive term of the change in matrix volume fraction in the governing equation represented by the balance of equilibrated forces. The system of ordinary differential equations of second order resulting from the balance of momentum is solved by the Houbolt finite-difference scheme as a time stepping method.

The rest of the paper is organized as follows; in Section 2, the governing equations for elastic materials with voids are presented. The derivation of the local integral equations is detailed in Section 3. Section 4 introduces the numerical solutions based on the moving least squares method. Some numerical examples are provided in Section 5 and conclusions are summarized in Section 6.

2. Governing equations for elastic materials with voids

The linear theory of elastic materials with voids deals with small changes from a reference configuration of a porous body. The matrix volume fraction at the strain-free state is denoted as κ_0. However, it does not mean that it has to correspond to a stress-free state necessarily. The considered theory asserts that the mass density ρ has the decomposition (Cowin and Nunziato, 1983), $\rho(\mathbf{x},\tau)=\kappa(\mathbf{x},\tau)\gamma$, where γ is the density of the matrix material, and κ $(0<\kappa\leq 1)$ is the matrix volume fraction field. The change in volume fraction from the reference volume fraction (also known as micro-dilatation or porosity change function), $\phi(\mathbf{x},\tau)$, is defined as

$$\phi(\mathbf{x},\tau)=\kappa(\mathbf{x},\tau)-\kappa_0(\mathbf{x}) \tag{1}$$

Then, the two independent kinematic variables in this linear theory are the displacement field $u_i(\mathbf{x},\tau)$ and the micro-dilatation field. The strain tensor $\varepsilon_{ij}(\mathbf{x},\tau)$ is determined from displacements:

$$\varepsilon_{ij}=\frac{1}{2}(u_{i,j}+u_{j,i}) \tag{2}$$

where $i, j=1,2,3$ for the 3D case and 1,.2 for the 2D case.

Governing equations for elastic medium with voids have to satisfy the balance of momentum

$$\sigma_{ij,j}+\rho b_i=\rho\ddot{u}_i \tag{3}$$

and the balance of equilibrated forces (Cowin and Nunziato, 1983)

$$h_{i,i}+g+\rho l=\rho k\ddot{\phi} \tag{4}$$

where σ_{ij} is the symmetric stress tensor, b_i is the body force vector, h_i is the equilibrated stress vector, k is the equilibrated inertia, g is the intrinsic equilibrated body force, and l is the extrinsic equilibrated body force.

The constitutive equations for the linear isotropic theory of elastic materials with voids relate the stress tensor σ_{ij}, the equilibrated stress vector h_i and the intrinsic equilibrated body force g to the strain ε_{ij}, the change in volume fraction ϕ, the time rate of change in volume fraction $\dot{\phi}$, and the gradient of the change in volume fraction $\psi_i=\phi_{,i}$ (Cowin and Nunziato, 1983) as

$$\sigma_{ij}=2\mu\varepsilon_{ij}+\lambda\delta_{ij}\varepsilon_{kk}+\beta\phi\delta_{ij}, \tag{5}$$

$$h_i=\alpha\psi_i, \tag{6}$$

$$g=-\omega\dot{\phi}-\xi\phi-\beta\varepsilon_{kk} \tag{7}$$

where coefficients μ, λ, α, β, ξ and ω depend on the reference volume fraction κ_0. Coefficients α,β,ξ represent material parameters related to porosity of the medium. Obviously, if $\beta=0$, mechanical displacements and micro-dilatation are independent fields.

For a unique solution of the considered coupled problem, the initial and boundary conditions should be specified. The following essential and natural boundary conditions are assumed for the mechanical fields

$$\begin{aligned} &u_i(\mathbf{x},\tau)=\tilde{u}_i(\mathbf{x},\tau) \quad \text{on} \quad \partial\Omega_u,\\ &t_i(\mathbf{x},\tau)\equiv\sigma_{ij}n_j=\tilde{t}_i(\mathbf{x},\tau) \quad \text{on} \quad \partial\Omega_t, \quad \partial\Omega=\partial\Omega_u\cup\partial\Omega_t, \end{aligned} \tag{8}$$

and the equilibrated stress vector boundary condition

$$h_i(\mathbf{x},\tau)n_i(\mathbf{x})=0 \quad \text{on} \quad \partial\Omega \tag{9}$$

where n_i is the unit normal vector to boundary $\partial\Omega$. The boundary condition (8) follows from the work of Adkin et al. (1977). This natural boundary condition means that there is no discontinuity in the surface flux of the quantity conserved in a direction normal to an external boundary.

3. Local integral equations

Consider an elastic body in a 2D domain Ω, with a boundary $\partial\Omega$. In MLPG approaches, one may write a weak form over a local subdomain Ω_s, which may have an arbitrary shape. The local weak form of the governing Eq. (3) can be written as (Atluri, 2004)

$$\int_{\Omega_s}[\sigma_{ij,j}(\mathbf{x},\tau)-\rho\ddot{u}_i(\mathbf{x},\tau)+\rho b_i(\mathbf{x},\tau)]\,u^*_{ik}(\mathbf{x})\,d\Omega=0, \tag{10}$$

where $u^*_{ik}(\mathbf{x})$ is a test function.

By applying the divergence theorem to the first integral one obtains

$$\begin{aligned} &\int_{\partial\Omega_s}\sigma_{ij}(\mathbf{x},\tau)n_j(\mathbf{x})u^*_{ik}(\mathbf{x})d\Gamma-\int_{\Omega_s}\sigma_{ij}(\mathbf{x},\tau)u^*_{ik,j}(\mathbf{x})d\Omega\\ &+\int_{\Omega_s}[-\rho\ddot{u}_i(\mathbf{x},\tau)+\rho b_i(\mathbf{x},\tau)]u^*_{ik}(\mathbf{x})d\Omega=0, \end{aligned} \tag{11}$$

where $\partial\Omega_s$ is the boundary of the local subdomain which consists of three parts $\partial\Omega_s=L_s\cup\Gamma_{st}\cup\Gamma_{su}$ (Atluri, 2004). Here, L_s is the local boundary that is totally inside the global domain, Γ_{st} is the part of the local boundary which coincides with the global traction boundary, i.e., $\Gamma_{st}=\partial\Omega_s\cap\partial\Omega_t$, and similarly Γ_{su} is the part of the local boundary that coincides with the global displacement boundary, i.e., $\Gamma_{su}=\partial\Omega_s\cap\partial\Omega_u$.

By choosing a Heaviside step function as the test function $u^*_{ik}(\mathbf{x})$ in each subdomain

$$u^*_{ik}(\mathbf{x})=\begin{cases}\delta_{ik} & \text{at} \quad \mathbf{x}\in\Omega_s\\ 0 & \text{at} \quad \mathbf{x}\notin(\Omega_s\cup\partial\Omega_s)\end{cases},$$

the local weak-form (11) is converted into the following local boundary-domain integral equations

$$\begin{aligned} &\int_{L_s+\Gamma_{su}}t_i(\mathbf{x},\tau)d\Gamma-\int_{\Omega_s}\rho\ddot{u}_i(\mathbf{x},\tau)d\Omega\\ &=-\int_{\Gamma_{st}}\tilde{t}_i(\mathbf{x},\tau)d\Gamma-\int_{\Omega_s}\rho b_i(\mathbf{x},\tau)d\Omega. \end{aligned} \tag{12}$$

Eq. (12) is recognized as the overall force equilibrium conditions on subdomain Ω_s. The traction vector inside the integral sign can be expressed by the constitutive Eq. (5)

$$t_i(\mathbf{x},\tau) = \sigma_{ij}(\mathbf{x},\tau)n_j(\mathbf{x}) = \mu(n_j(\mathbf{x})u_{i,j}(\mathbf{x},\tau) + n_j(\mathbf{x})u_{j,i}(\mathbf{x},\tau)) + \lambda n_i(\mathbf{x})u_{j,j}(\mathbf{x},\tau) + \beta n_i(\mathbf{x})\phi(\mathbf{x},\tau).$$

Similarly, the local weak-form of the governing Eq. (4) representing the balance of equilibrated forces is given by

$$\int_{\Omega_s} [h_{i,i}(\mathbf{x},\tau) - \omega\dot{\phi}(\mathbf{x},\tau) - \xi\phi(\mathbf{x},\tau) - \beta u_{i,i}(\mathbf{x},\tau) + \rho l(\mathbf{x},\tau) - \rho k\ddot{\phi}(\mathbf{x},\tau)]v^*(\mathbf{x})\, d\Omega = 0, \tag{13}$$

where $v^*(\mathbf{x})$ is a test function. The definition of g in Eq. (7) was used in the above equation.

Applying Gauss divergence theorem to the local weak-form (13) and choosing the Heaviside step function as the test function $v^*(\mathbf{x})$, one can obtain

$$\int_{\partial\Omega_s} q(\mathbf{x},\tau)d\Gamma - \int_{\Omega_s} [\omega\dot{\phi}(\mathbf{x},\tau) + \xi\phi(\mathbf{x},\tau) + \beta u_{i,i}(\mathbf{x},\tau) - \rho l(\mathbf{x},\tau) + \rho k\ddot{\phi}(\mathbf{x},\tau)], d\Omega = 0, \tag{14}$$

where

$$q(\mathbf{x},\tau) = h_j(\mathbf{x},\tau)n_j(\mathbf{x}) = \alpha n_j(\mathbf{x})\phi_{,j}(\mathbf{x},\tau).$$

It should be noted that q on an artificial boundary $\partial\Omega_s$ is not vanishing. It vanishes only on the global boundary $\partial\Omega$ as it follows from boundary condition (9).

4. Moving least square approximation

The MLS is generally considered to be one of the best meshless schemes to approximate quantities with high accuracy, and the desired completeness and continuity. A number of nodes spread over the domain of influence are used for the approximation of a field. The trial function $\mathbf{u}(\mathbf{x},\tau)$ at any point $\mathbf{x}$ may be defined by (Lancaster and Salkauskas, 1981; Nayroles et al., 1992; Atluri, 2004)

$$\mathbf{u}^h(\mathbf{x},\tau) = \sum_{i=1}^{m} p_i(\mathbf{x})a_i(\mathbf{x},\tau) = \mathbf{p}^T(\mathbf{x})\mathbf{a}(\mathbf{x},\tau), \tag{15}$$

where $\mathbf{p}^T(\mathbf{x}) = \{p_1(\mathbf{x}), p_2(\mathbf{x}), \dots p_m(\mathbf{x})\}$ is a vector of complete basis functions of order m and $\mathbf{a}(\mathbf{x},\tau) = \{a_1(\mathbf{x},\tau), a_2(\mathbf{x},\tau), \dots a_m(\mathbf{x},\tau)\}$ is a vector of unknown parameters that depend on $\boldsymbol{x}$. For example, in 2-D problems

$$\mathbf{p}^T(\mathbf{x}) = \{1, x_1, x_2\} \quad \text{for} \quad m = 3$$

and

$$\mathbf{p}^T(\mathbf{x}) = \{1, x_1, x_2, x_1^2, x_1x_2, x_2^2\} \quad \text{for} \quad m = 6$$

are linear and quadratic basis functions, respectively.

The vector of function $\mathbf{a}(\mathbf{x},\tau)$ is determined by minimizing a weighted discrete L_2 norm

$$J[\mathbf{a}(\mathbf{x},\tau)] = \sum_{a=1}^{n} w^a(\mathbf{x})[\mathbf{p}^T(\mathbf{x}^a)\mathbf{a}(\mathbf{x},\tau) - \hat{u}^a(\tau)]^2, \tag{16}$$

where n is the number of nodes used for the approximation. It is determined by the weight function $w^a(\mathbf{x})$ associated with the node a. The symbol $\hat{u}^a(\tau)$ stands for the fictitious nodal values, but not the nodal values of the unknown trial functions in general. The stationarity of J in Eq. (16) with respect to $\mathbf{a}(\mathbf{x},\tau)$ leads to the following linear relation between $\mathbf{a}(\mathbf{x},\tau)$ and $\hat{u}(\tau) = [\hat{u}^1(\tau), \dots, \hat{u}^n(\tau)]^T$

$$\mathbf{A}(\mathbf{x})\mathbf{a}(\mathbf{x},\tau) - \mathbf{B}(\mathbf{x})\hat{u}(\tau) = 0, \tag{17}$$

where

$$\mathbf{A}(\mathbf{x}) = \sum_{a=1}^{n} w^a(\mathbf{x})\mathbf{p}(\mathbf{x}^a)\mathbf{p}^T(\mathbf{x}^a),$$

$$\mathbf{B}(\mathbf{x}) = [w^1(\mathbf{x})\mathbf{p}(\mathbf{x}^1), w^2(\mathbf{x})\mathbf{p}(\mathbf{x}^2), \dots, w^n(\mathbf{x})\mathbf{p}(\mathbf{x}^n)]. \tag{18}$$

The solution of Eq. (17) for $\mathbf{a}(\mathbf{x},\tau)$ and the subsequent substitution into Eq. (15) gives the approximate formulas for the mechanical displacements, and micro-dilatation

$$\mathbf{u}^h(\mathbf{x},\tau) = \mathbf{N}^T(\mathbf{x})\cdot\hat{\mathbf{u}} = \sum_{a=1}^{n} N^a(\mathbf{x})\hat{\mathbf{u}}^a(\tau),$$

$$\phi^h(\mathbf{x},\tau) = \sum_{a=1}^{n} N^a(\mathbf{x})\hat{\phi}^a(\tau), \tag{19}$$

where the nodal values $\hat{\mathbf{u}}^a(\tau) = (\hat{u}_1^a(\tau), \hat{u}_2^a(\tau))^T$ and $\hat{\phi}^a(\tau)$ are fictitious parameters for displacements, and micro-dilatation, respectively, and $N^a(\mathbf{x})$ is the shape function associated with node a. The number of nodes n used for the approximation is determined by the weight function $w^a(\mathbf{x})$. A 4th order spline-type weight function is applied in the present work

$$w^a(\mathbf{x}) = \begin{cases} 1 - 6\left(\frac{d^a}{r^a}\right)^2 + 8\left(\frac{d^a}{r^a}\right)^3 - 3\left(\frac{d^a}{r^a}\right)^4, & 0 \le d^a \le r^a \\ 0, & d^a \ge r^a \end{cases}, \tag{20}$$

where $d^a = \|\mathbf{x} - \mathbf{x}^a\|$, and r^a is the radius of the support domain. It is seen that the C^1-continuity is ensured over the entire domain, and therefore continuity conditions of tractions, and equilibrated stress vector are satisfied. A necessary condition for a regular MLS approximation is that at least m weight functions are non-zero (i.e. $n \ge m$) for each sample point $\mathbf{x} \in \Omega$. This condition determines the size of the support domain.

Then, the traction vector $t_i(\mathbf{x},\tau)$ at a boundary point $\mathbf{x} \in \partial\Omega_s$ is approximated in terms of the same nodal values $\hat{\mathbf{u}}^a(\tau)$ as

$$\mathbf{t}^h(\mathbf{x},\tau) = \mathbf{O}(\mathbf{x})\mathbf{C}\sum_{a=1}^{n}\mathbf{B}^a(\mathbf{x})\hat{\mathbf{u}}^a(\tau) + \beta\mathbf{O}_1(\mathbf{x})\sum_{a=1}^{n}N^a(\mathbf{x})\hat{\phi}^a(\tau), \tag{21}$$

where the matrix $\mathbf{O}(\mathbf{x})$ is related to the normal vector $\mathbf{n}(\mathbf{x})$ on $\partial\Omega_s$ by

$$\mathbf{O}(\mathbf{x}) = \begin{bmatrix} n_1 & 0 & n_2 \\ 0 & n_2 & n_1 \end{bmatrix}, \quad \mathbf{C} = \begin{bmatrix} 2\mu+\lambda & \lambda & 0 \\ \lambda & 2\mu+\lambda & 0 \\ 0 & 0 & \mu \end{bmatrix},$$

$$\mathbf{O}_1(\mathbf{x}) = \begin{bmatrix} n_1 \\ n_2 \end{bmatrix},$$

and finally, the matrix $\mathbf{B}^a$ is represented by the gradients of the shape functions as

$$\mathbf{B}^a(\mathbf{x}) = \begin{bmatrix} N^a_{,1} & 0 \\ 0 & N^a_{,2} \\ N^a_{,2} & N^a_{,1} \end{bmatrix}.$$

The scalar product of the equilibrated stress vector $q(\mathbf{x},\tau)$ is approximated by

$$q^h(\mathbf{x},\tau) = \alpha n_i\sum_{a=1}^{n}N^a_{,i}(\mathbf{x})\hat{\phi}^a(\tau) = \alpha\mathbf{O}_1^T(\mathbf{x})\sum_{a=1}^{n}\mathbf{P}^a(\mathbf{x})\hat{\phi}^a(\tau), \tag{22}$$

where

$$\mathbf{P}^a(\mathbf{x}) = [N^a_{,1} \quad N^a_{,2}]^T.$$

Satisfying the essential boundary conditions and making use of the approximation formulae (19), one obtains the discretized form of these boundary conditions as

$$\sum_{a=1}^{n}N^a(\zeta)\hat{\mathbf{u}}^a(\tau) = \tilde{\mathbf{u}}(\zeta,\tau) \quad \text{for} \quad \zeta \in \Gamma_u, \tag{23}$$

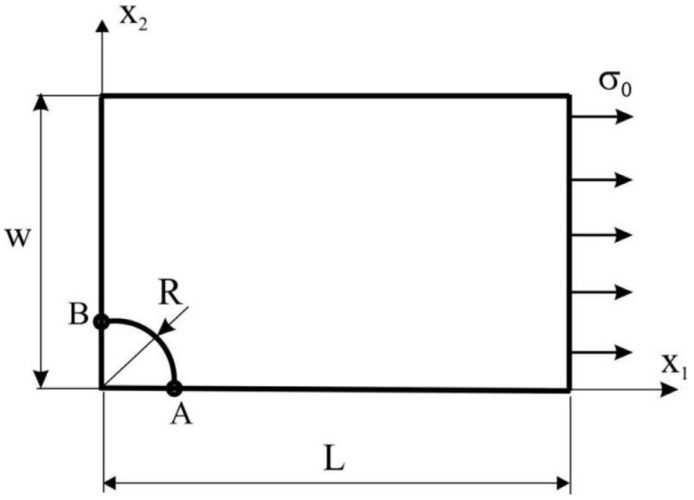

Fig. 1. Quarter of rectangular plate with a circular hole.

Furthermore, in view of the MLS-approximations (21–22) for the unknown quantities in the local boundary-domain integral Eqs. (12), and (14), one obtains their discretized forms as

$$\sum_{a=1}^{n}\left[\left(\int_{L_s}\mathbf{O}(\mathbf{x})\mathbf{C}\mathbf{B}^a(\mathbf{x})d\Gamma\right)\hat{\mathbf{u}}^a(\tau)-\left(\int_{\Omega_s}\rho N^a d\Omega\right)\ddot{\hat{\mathbf{u}}}^a(\tau)\right]$$
$$+\sum_{a=1}^{n}\left(\int_{L_s}\beta\mathbf{O}_1(\mathbf{x})N^a(\mathbf{x})d\Gamma\right)\hat{\phi}^a(\tau)$$
$$=-\int_{\Gamma_{st}}\tilde{\mathbf{t}}(\mathbf{x},\tau)d\Gamma-\int_{\Omega_s}\rho\mathbf{b}(\mathbf{x},\tau)d\Omega, \tag{24}$$

$$\sum_{a=1}^{n}\left[\left(\alpha\int_{L_s}\mathbf{O}_1^T(\mathbf{x})\mathbf{P}^a(\mathbf{x})d\Gamma\right)\hat{\phi}^a(\tau)-\left(\int_{\Omega_s}\rho k N^a(\mathbf{x})d\Gamma\right)\ddot{\hat{\phi}}^a(\tau)\right]$$
$$-\sum_{a=1}^{n}\left(\int_{\Omega_s}\omega N^a(\mathbf{x})d\Gamma\right)\dot{\hat{\phi}}^a(\tau)-\sum_{a=1}^{n}\left(\int_{\Omega_s}\xi N^a(\mathbf{x})d\Omega\right)\hat{\phi}^a(\tau)$$
$$-\sum_{a=1}^{n}\left(\int_{\Omega_s}\beta\mathbf{P}^{aT}(\mathbf{x})d\Omega\right)\hat{\mathbf{u}}^a(\tau)=-\int_{\Omega_s}\rho l(\mathbf{x},\tau)d\Omega, \tag{25}$$

where Eq. (24) is considered on sub-domains adjacent to the interior nodes as well as to boundary nodes on Γ_{st}, while Eq. (25) on sub-domains of each node, because of the boundary condition (9).

Collecting the discretized local boundary-domain integral equations together with the discretized boundary conditions for the displacements, results in a complete system of ordinary differential equations which can be rearranged in such a way that all known quantities are on the r.h.s. Thus, in matrix form, the system becomes

$$\mathbf{A}\ddot{\mathbf{x}}+\mathbf{B}\dot{\mathbf{x}}+\mathbf{C}\mathbf{x}=\mathbf{Y}. \tag{26}$$

There are many time integration procedures for solving this system of ordinary differential equations. In the present work, the Houbolt method is applied. In the Houbolt finite- difference scheme (Houbolt, 1950), the "acceleration" ($\ddot{\mathbf{x}}^a\in\{\ddot{\hat{\mathbf{u}}}^a,\ddot{\hat{\phi}}^a\}$) is expressed as

$$\ddot{\mathbf{x}}_{\tau+\Delta\tau}=\frac{2\mathbf{x}_{\tau+\Delta\tau}-5\mathbf{x}_{\tau}+4\mathbf{x}_{\tau-\Delta\tau}-\mathbf{x}_{\tau-2\Delta\tau}}{\Delta\tau^2}, \tag{27}$$

where $\Delta\tau$ is the time step. The backward difference method is applied for the approximation of "velocities"

$$\dot{\mathbf{x}}_{\tau+\Delta\tau}=\frac{\mathbf{x}_{\tau+\Delta\tau}-\mathbf{x}_{\tau}}{\Delta\tau}. \tag{28}$$

Substituting Eqs. (27) and (28) into Eq. (26), we get the following system of algebraic equations for the unknowns $\mathbf{x}_{\tau+\Delta\tau}$

$$\left[\frac{2}{\Delta\tau^2}\mathbf{A}+\frac{1}{\Delta\tau}\mathbf{B}+\mathbf{C}\right]\mathbf{x}_{\tau+\Delta\tau}$$
$$=\frac{1}{\Delta\tau^2}(5\mathbf{A}+\mathbf{B}\Delta\tau)\mathbf{x}_{\tau}+\mathbf{A}\frac{1}{\Delta\tau^2}\{-4\mathbf{x}_{\tau-\Delta\tau}+\mathbf{x}_{\tau-2\Delta\tau}\}+\mathbf{Y}. \tag{29}$$

The value of the time step has to be appropriately selected with respect to material parameters (wave velocities) and time dependence of the boundary conditions.

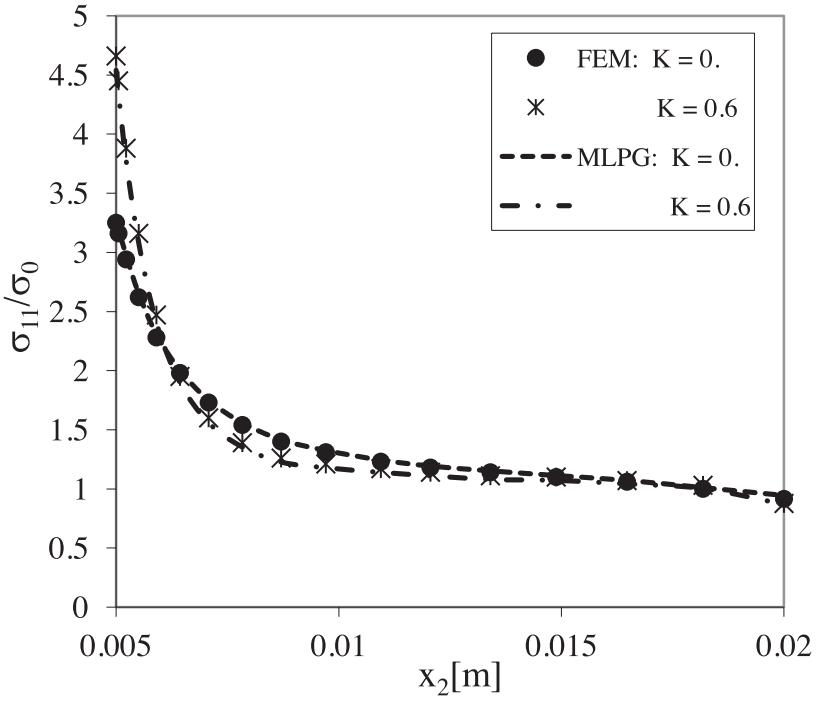

Fig. 2. Variation of stress component σ_{11} along x_2-axis for various values of K.

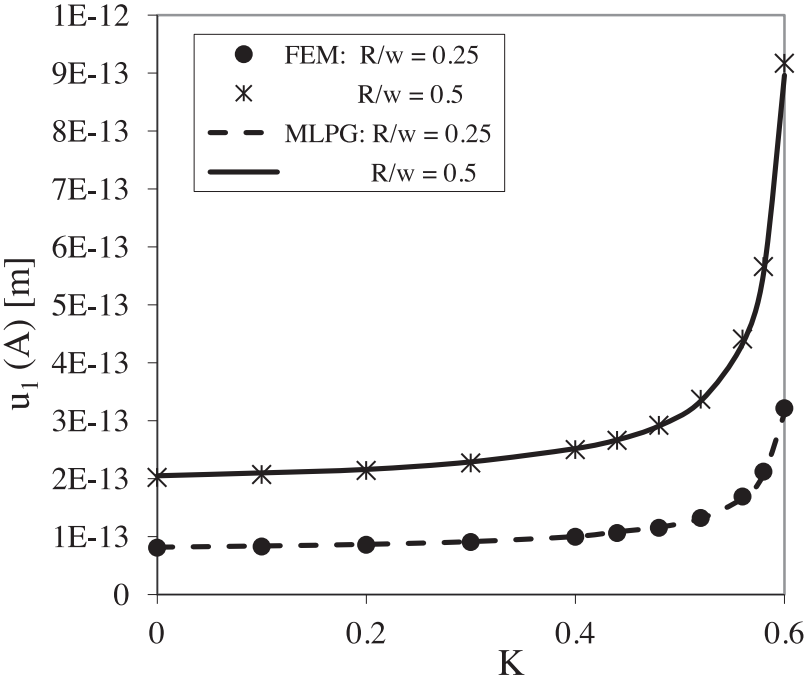

Fig. 3. Influence of the dimensionless parameter K on the displacement u_1 at point A.

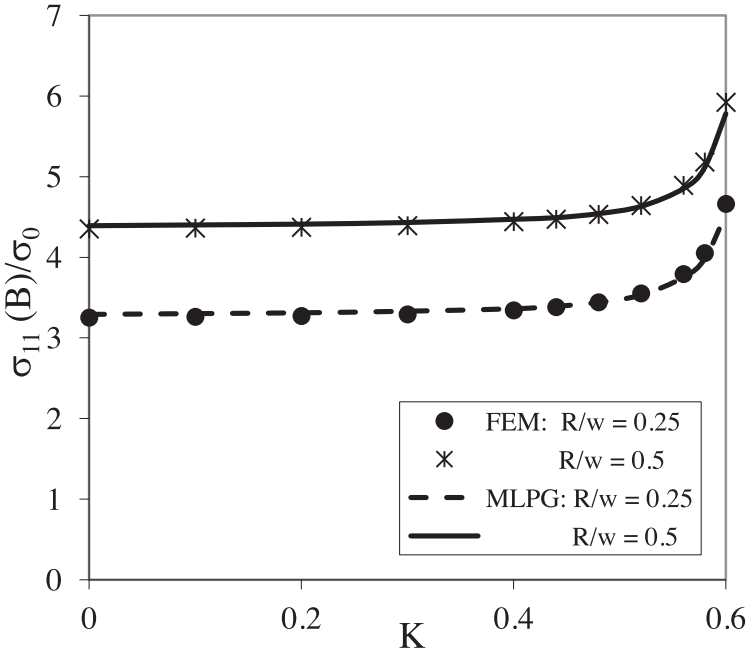

Fig. 4. Influence of the dimensionless parameter K on the stress σ_{11} at point B.

5. Numerical examples

5.1. Rectangular plate with a circular hole (Kirsch's problem)

The static problem of uniaxial tension on a rectangular plate with a circular hole (Kirsch's problem) is analyzed to verify accuracy of the present computational method. The same problem has been analyzed by the FEM (Iovane and Nasedkin, 2005). The geometric parameters are illustrated in Fig. 1.

The length of the specimen is considered as $L = 0.05m$ and width $w = 0.02m$. Various ratios of the radius of the hole to the plate width R/w are considered. The material parameters were taken as follows: Young's modulus $E = 2 \cdot 10^{11} N/m^2$, Poisson ratio $\nu = 0.3$, parameters related to porosity of the medium $\alpha = 0.01N$ and $\xi = 6 \cdot 10^4 N/m^2$. The coefficient β is determined by the dimensionless coupling parameter

$$K = \frac{\beta^2}{\xi(2\mu + \lambda)}. \tag{30}$$

Lame's parameters for an isotropic material are easily expressed through Young's modulus and Poisson's ratio as:

$$\mu = \frac{E}{2(1+\nu)}; \quad \lambda = \frac{E\nu}{(1+\nu)(1-2\nu)}. \tag{31}$$

In numerical analyses we have used 390 nodes with an irregular distribution like Atluri et al. (2006) for a similar problem in

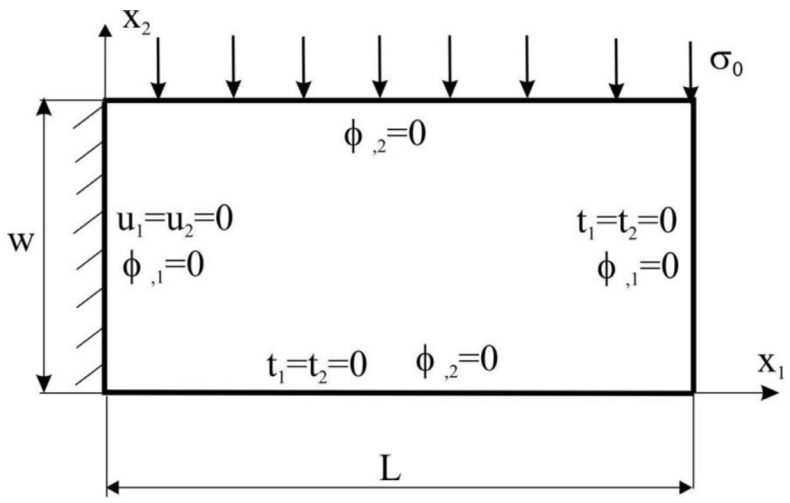

Fig. 5. A cantilever beam.

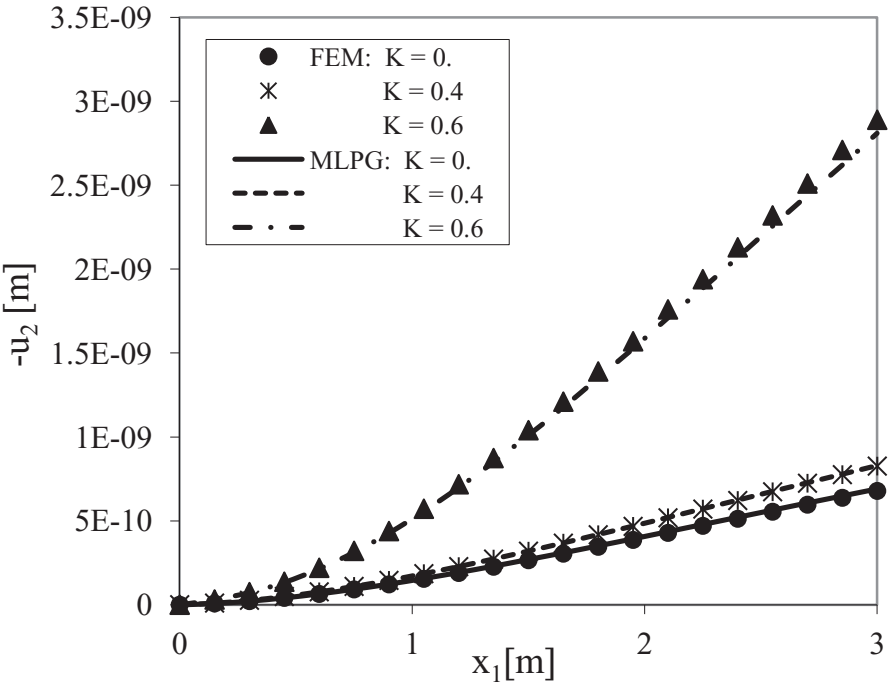

Fig. 6. Variation of beam deflection along x_1-axis for various values of K.

classical linear elasticity. A uniform tension stress $\sigma_0 = 1Pa$ is considered. All body forces are vanishing ($b_i = l = 0$). One can observe that the stress concentration around the hole in elastic material with voids exceeds the stress concentration around the hole in homogeneous elastic material (Fig. 2). The influence of the dimensionless coupling parameter K on the displacement u_1 and stress σ_{11} for two different ratios R/w is presented in Figs. 3 and 4. Very good agreement between MLPG and FEM results can be seen. The FEM results have been obtained using COMSOL Multiphysics software package with 1107 triangular elements with Lagrange approximation of the second order.

As the radius of the hole grows with respect to the plate width the stress concentration at point B increases. However, the influence of the dimensionless parameter K is the same for both ratios $R/w = 0.25$ and 0.5. Almost parallel curves for displacement and stress can be seen in Figs. 3 and 4, respectively.

5.2. Analysis of a cantilever beam

A cantilever beam under uniform normal load on the upper surface is analyzed in the second example (Fig. 5). Plane stress conditions are considered. The same material parameters are used as in the previous example. The following geometry is considered: length of the beam $L = 3$ m, height $w = 1$ m.

A regular distribution of 341 ($31 \times 11 = 341$) nodes is considered in numerical analyses. The variation of the beam deflection at the neutral axis ($x_2 = w/2$) along x_1-axis is presented in Fig. 6. One can observe that the deflection of a beam of elastic material with voids exceeds the deflection of a beam of homogeneous elastic material. The effect of increasing the coupling parameter, K, on the beam deflection increase is nonlinear. Again very good agreement between MLPG and FEM results can be seen. The FEM results have been obtained using COMSOL Multiphysics software package with 672 triangular elements.

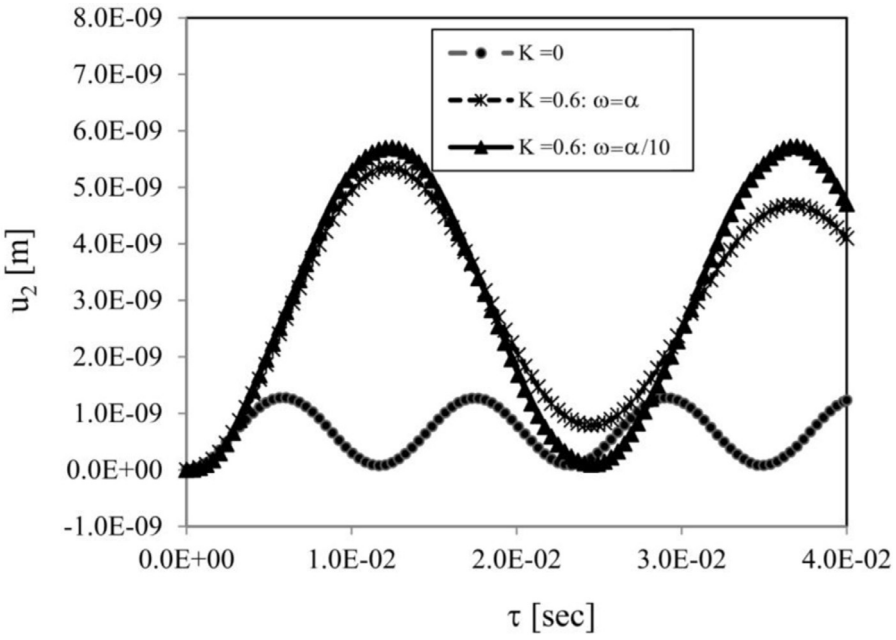

Fig. 7. Time variation of the beam deflection at $x_1 = L$ for various values of K.

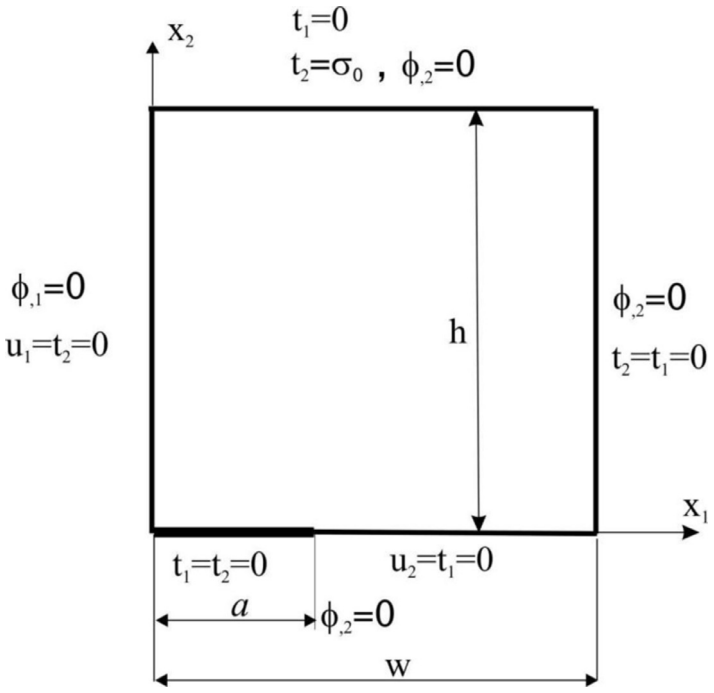

Fig. 8. Central crack in a finite strip with voids.

The same beam is analyzed under impact load with Heaviside time variation. The additional material coefficients are considered as in Puri and Cowin (1985): the mass density $\rho = 7500 kg/m^3$ and two different values of ω: $\omega = \alpha/10$, $\omega = \alpha$. The inertial coefficient for the change in volume fraction is vanishing ($k = 0$). The same node distribution for approximation of fields is used as in the static case.

One can observe in Fig. 7 that amplitudes of the beam deflection are approximately doubled with respect to static values (see Fig. 6, where $u_2 = 0.285 \cdot 10^{-9} m$ for $K = 0.6$). The parameter ω is responsible for damping. With increasing the value of ω, the amplitude decreases with time.

5.3. Analysis of porous finite strip with central crack

Let us consider a central straight crack of length $2a$ in the considered porous finite strip with a uniform tension σ_0 acting on the top and bottom surfaces (see Fig. 8). The geometry of the strip has the following values: $a = 0.5$m, $a/w = 0.4$ and $h/w = 1.2$. Due to the symmetry of the problem with respect to both Cartesian coordinates, only a quarter of the strip is modeled. All body forces are vanishing ($b_i = l = 0$).

The displacements and micro-dilatation on the finite strip are approximated using 930 (31×30) equidistantly distributed nodes. The local subdomains are selected to be circular with radius

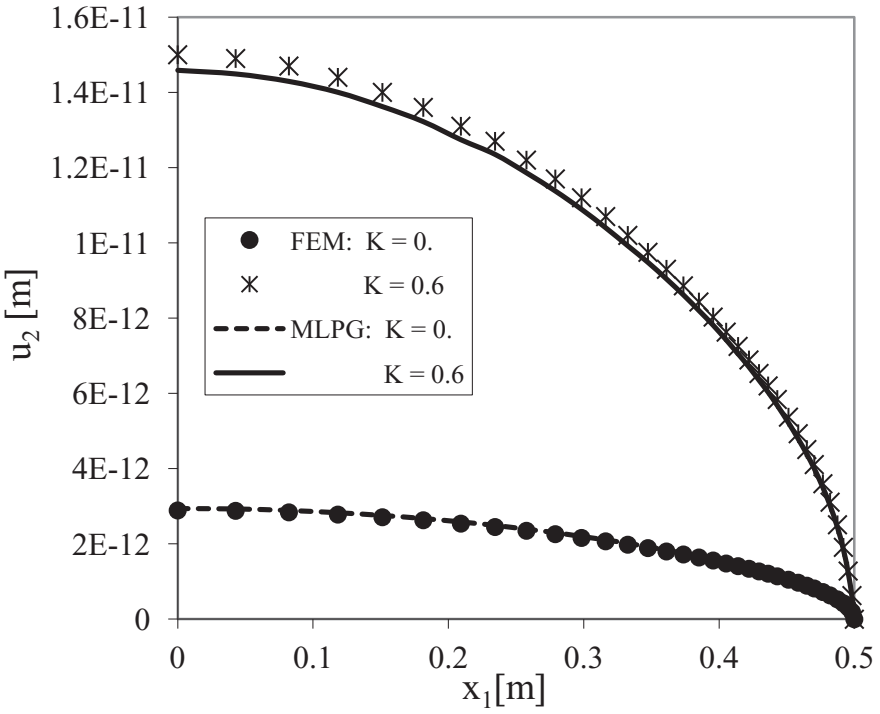

Fig. 9. Crack opening displacement along the crack.

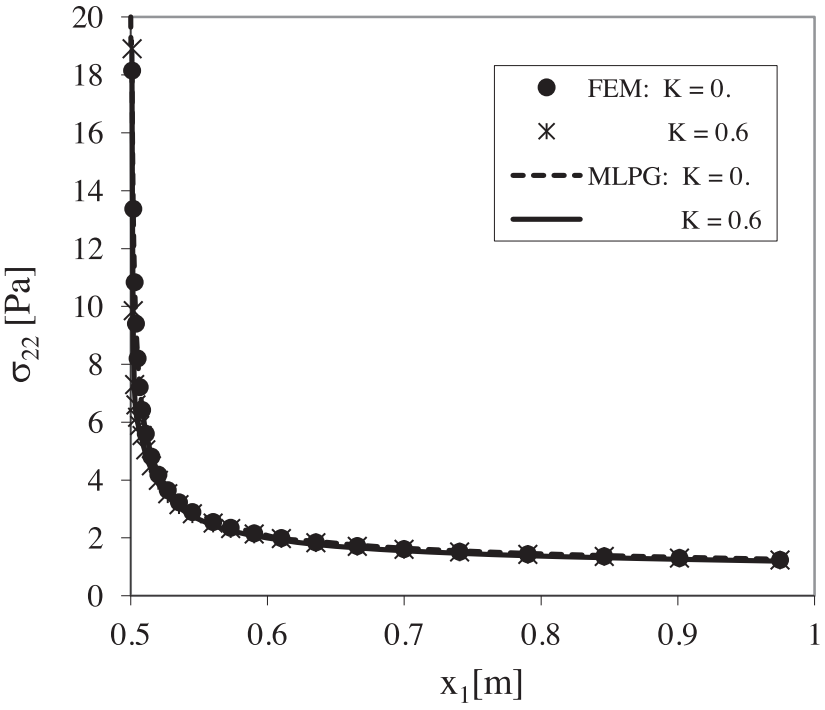

Fig. 10. Variation of the stress σ_{22} ahead of the crack tip.

$r_{loc} = 0.028m$. The FEM results are obtained using COMSOL Multiphysics software package with 3595 triangular (6-node) elements. The crack opening displacement for a uniform load $\sigma_0 = 1Pa$ is presented in Fig. 9. A very good agreement can be seen between MLPG and FEM results. A small discrepancy less than 2% appears for porous elastic material with corresponding coupling number $K = 0.6$. Furthermore, a significant increase of the crack opening displacement is observed with increasing porosity (dimensionless coupling parameter K). This observation is opposite to that in (Popuzin and Pennisi 2014). Extending the observation of the previous examples to crack problems, the stiffness of a porous medium decreases, and displacements should grow with higher porosity.

Ciarletta et al. (2003) showed that the singular behavior at the crack tip for a finite crack in an infinite medium described by micro-dilatation theory is the same as in conventional elasticity. This observation is not surprising, since the media with voids considered within the Cowin-Nunziato theory is a continu-

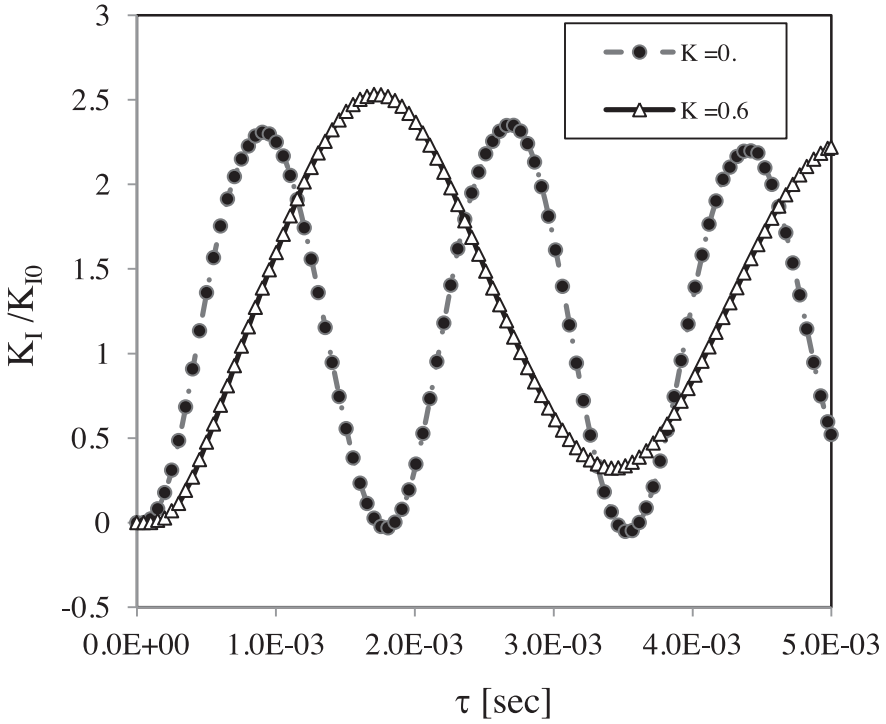

Fig. 11. Time variation of the normalized SIF for cracked specimen under impact load.

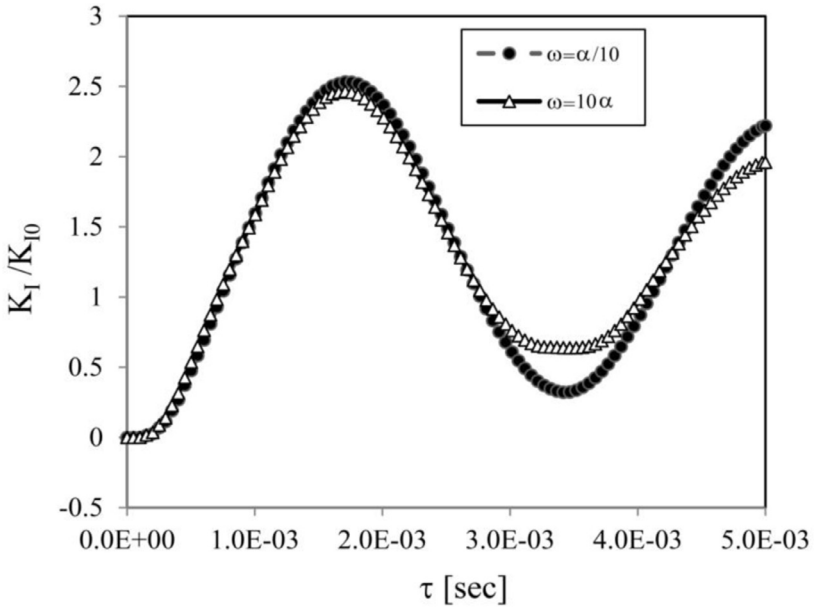

Fig. 12. Influence of material parameter ω on the amplitudes of SIF for cracked specimen under impact load.

ous media without modeling any discontinuous material nonhomogeneities, and the influence of voids is taken into account via the porosity change function, equilibrated stresses and forces. Thus, stresses exhibit $1/\sqrt{r}$ behavior, where r is the radial polar coordinate with origin at the crack tip. Therefore the stress intensity factor (SIF) for the first mode is defined like in classical fracture mechanics

$$K_I = \lim_{r\to 0} \sqrt{2\pi r}\sigma_{22}(r,0)\,. \tag{32}$$

Thus, the stress field near the crack tip vicinity is a product of two factors: (i) the SIF which is dependent on the solution of the boundary value problem (b.v.p.) and material coefficients; (ii) the singular factor $1/\sqrt{r}$ which is the same for any elastic continuous media and independent on the b.v.p. The stress intensity factor of pure mode I for the considered boundary conditions is $K_I^{class} = 1.42\text{Pa}\cdot\text{m}^{1/2}$ for classical elastic material ($K=0$). This value is computed from Eq. (30) by extrapolating the near-field quantities (σ_{22}) ahead of the crack tip. The variation of the stress component σ_{22} ahead the crack tip is presented in Fig. 10. The stress values in the porous material ($K=0.6$) are larger than that in the same material without pores ($K=0$). Obviously, the larger values of σ_{22} obtained from the numerical solution of the considered b.v.p. in the porous medium with $K=0.6$ yield larger value of SIF $K_I^{K=0.6} = 1.56\ \text{Pa}\cdot\text{m}^{1/2}$.

The same cracked specimen under an impact load with Heaviside time variation is analyzed too. The additional material coefficients are considered as: mass density $\rho = 7500kg/m^3$ and $\omega = \alpha/10$. The SIF is normalized by $K_{I0} = \sigma_0\sqrt{\pi a}$. The time variation of the normalized SIF for porous and non-porous medium is presented in Fig. 11. One can observe that the peak of the SIF for porous medium is a little bit larger than that in non-porous one. The same amplification of SIF in porous medium has been observed in static case. The peak value in porous medium is shifted to larger time instants. This predicted slower propagation of elastic waves in porous medium which is consistent with the concept of softening the continuous medium with increasing porosity. The value of the parameter ω has an influence on the damping of the SIF amplitudes. With increasing the value of ω parameter the level of damping is increasing (see Fig. 12).

6. Conclusions

An MLPG model is successfully developed for coupled partial differential equations describing elasticity problems in a medium with voids. The mechanical displacements and the micro-dilatation (change in matrix volume fraction from a reference state) fields are coupled via the constitutive equations in Cowin-Nunziato theory. The influence of porosity on the stress concentration factor is investigated. The stress concentration factor in the case of medium with voids is always higher than that in the case of elastic medium without voids. This is consistent with the concept of voids in the skeleton, where stress transfer is possible only through the skeleton, and therefore stresses in the skeleton are increasing with increasing porosity. In the case of crack problems, the amplification of stress concentration (represented by the stress intensity factor) is only about 10% for medium with dimensionless porosity parameter K = 0.6. Recall that there is a singular concentration of stresses near the crack tip and the amplification of huge stresses must be limited because of the energetic balance. The parameter ω in Cowin-Nunziato theory has a damping effect in dynamic problems. With increasing the value of ω, the amplitude decreases with time. The propagation of elastic waves in a porous medium is slower than that in the same material without pores.

Acknowledgment

The first and third authors acknowledge the support by the Slovak Science and Technology Assistance Agency registered under number APVV-14-0216. The generous support of California State University, Northridge (CSUN) to the fourth author is also acknowledged.

References

Ashby, M.F., Evans, A.G., Fleck, N.A., Gibson, L.J., Hutchinson, J.W., Wadley, H.N.G., 2000. Metal Foams: A Design Guide. Butterworth Heinemann, Oxford.
Adkin, R.J., Cowin, S.C., Fox, N., 1977. On boundary conditions for polar materials. ZAMP 28, 1017–1026.
Atluri, S.N., Shen, S.P., 2002. The meshless local Petrov-Galerkin (MLPG) method: a simple & less costly alternative to the finite element and boundary element methods. CMES: Comput. Model. Eng. Sci. 3, 11–51.
Atluri, S.N., Han, Z.D., Shen, S.P., 2003. Meshless local Petrov-Galerkin (MLPG) approaches for solving the weakly-singular traction & displacement boundary integral equations. CMES: Comput. Model. Eng. Sci. 4, 507–516.
Atluri, S.N., 2004. The Meshless Method, (MLPG) for Domain & BIE Discretizations. Tech. Sci. Press.
Atluri, S.N., Liu, H.T., Han, Z.D., 2006. Meshless local Petrov-Galerkin (MLPG) mixed collocation method for elasticity problems. CMES: Comput. Model. Eng. Sci. 14, 141–152.
Biot, M.A., Willis, D.G., 1957. Elastic coefficients of the theory of consolidation. J. Appl. Mech. 24, 594–601.
Ciarletta, M., Iovane, G., Sumbatyan, M.A., 2003. On stress analysis for cracks in elastic materials with voids. Int. J. Eng. Sci. 41, 2447–2461.
Chandrasekharaiah, D.S., 1987. Effects of surface stresses and voids on Rayleigh waves in an elastic solid. Int. J. Eng. Sci. 25, 205–211.
Colombo, P.K., Scheffler, M. (Eds) 2005. Cellular Ceramics. Wiley-VCH, Weinheim.
Cowin, S.C., Nunziato, J.W., 1983. Linear elastic materials with voids. J. Elasticity 13, 125–147.
Han, Z.D., Atluri, S.N., 2004a. Meshless local Petrov-Galerkin (MLPG) approaches for solving 3D problems in elasto-statics. CMES: Comput. Model. Eng.. Sci. 6, 169–188.
Han, Z.D., Atluri, S.N., 2004b. A meshless local Petrov-Galerkin (MLPG) approach for 3-dimensional elasto-dynamics. CMC: Comput. Mater. Continua. 1, 129–140.
Houbolt, J.C., 1950. A recurrence matrix solution for the dynamic response of elastic aircraft. J. Aeronaut. Sci. 17, 371–376.
Iovane, G., Nasedkin, A.V., 2005. Finite element analysis of static problems for elastic media with voids. Comput. Struct. 84, 19–24.
Lancaster, P., Salkauskas, K., 1981. Surfaces generated by moving least square methods. Math. Comput. 37, 141–158.
Nayroles, B., Touzot, G., Villon, P., 1992. Generalizing the finite element method. Comput. Mech. 10, 307–318.
Popuzin, V., Pennisi, M., 2014. Fast numerical method for crack problem in the porous elastic material. Meccanica 49, 2169–2179.
Puri, P., Cowin, S.C., 1985. Plane waves in linear elastic materials with voids. J. Elasticity 15, 167–183.
Ramézani, H., Steeb, H., Jeong, J., 2012. Analytical and numerical studies on Penalized Micro-Dilatation (PMD) theory: macro-micro link concept. Eur. J. Mech. A/Solids 34, 130–148.
Ramézani, H., Jeong, J., 2015. Non-linear elastic micro-dilatation theory: matrix exponential function paradigm. Int. J. Solids Struct. 67-68, 1–26.
Scalia, A., Sumbatyan, M.A., 2000. Contact problem for porous elastic half-plane. J. Elasticity 60, 91–102.
Scalia, A., 2002. Contact problem for porous elastic strip. Int. J. Eng. Sci. 40, 401–410.
Shirzadi, A., Sladek, V., Sladek, J., 2013. A meshless simulations for 2D nonlinear reaction-diffusion Brusselator system. CMES - Comput. Model. Eng. Sci. 95, 259–282.
Sladek, J., Sladek, V., Atluri, S.N., 2004. Meshless local Petrov-Galerkin method in anisotropic elasticity. CMES: Comput. Model. Eng. Sci. 6, 477–489.
Sladek, J., Sladek, V., Zhang, Ch., Solek, P., 2007. Application of the MLPG to thermo-piezoelectricity. CMES - Comput. Model. Eng. Sci. 22, 217–233.
Sladek, J., Sladek, V., Solek, P., Wen, P.H., 2008a. Thermal bending of Reissner–Mindlin plates by the MLPG. CMES - Comput. Model. Eng. Sci. 28, 57–76.
Sladek, J., Sladek, V., Solek, P., Wen, P.H., Atluri, S.N., 2008b. Thermal analysis of Reissner-Mindlin shallow shells with FGM properties by the MLPG. CMES - Comput. Model. Eng. Sci. 30, 77–97.
Sladek, J., Sladek, V., Solek, P., Pan, E., 2008c. Fracture analysis of cracks in magneto-electro-elastic solids by the MLPG. Comput. Mech. 42, 697–714.
Sladek, V., Sladek, J., Zhang, Ch., 2008d. Computation of stresses in non-homogeneous elastic solids by local integral equation method: a comparative study. Comput. Mech. 41, 827–845.
Sladek, J., Sladek, V., Solek, P., 2009. Elastic analyses in 3D anisotropic functionally graded solids by the MLPG. CMES - Comput. Model. Eng. Sci. 43, 223–251.
Sladek, J., Stanak, P., Han, Z.D., Sladek, V., Atluri, S.N., 2013. Applications of the MLPG method in engineering & sciences: a review. CMES - Comput. Model. Eng. Sci. 92, 423–475.
Sladek, J., Sladek, V., Pan, E., Young, D.L., 2014. Dynamic anti-plane crack analysis in functionally graded piezoelectric semiconductor crystal. CMES - Comput. Model. Eng. Sci. 99, 273–296.